Journal of The Electrochemical Society, **162** (14) F1540-F1548 (2015)
0013-4651/2015/162(14)/F1540/9/$33.00 © The Electrochemical Society

Electrochemical Oxidation of Methanol on Pt-SnO_x/C Catalysts Characterized by Electrochemistry Methods

Xigui Sun,[a] Kewei Gao,[a] Xiaolu Pang,[a,z] Huisheng Yang,[a] and Alex A. Volinsky[b]

[a]*Department of Materials Physics and Chemistry, University of Science and Technology Beijing, Beijing 100083, People's Republic of China*
[b]*Department of Mechanical Engineering, University of South Florida, Tampa, Florida 33620, USA*

Pt-SnO_x/C catalysts with Pt/Sn atomic ratio of 1:1, 2:1, 3:1, 4:1 and 5:1 were prepared by the impregnation method. The electrochemical process of methanol oxidation on these five catalysts was studied using cyclic voltammetry and electrochemical impedance spectroscopy two simple real-time methods. Impregnation is a stable way to prepare Pt-SnO_x/C catalysts with accurate stoichiometry and uniform particle size, which increased from 3.8 nm to 5.4 nm as the Sn content decreased. The maximum current density of methanol electrochemical oxidation initially increased and then decreased with the Sn content, and Pt_3-SnO_x/C exhibited the highest value of about 16.6 mA · cm^{-2}. Methanol electrochemical oxidation on the Pt-SnO_x/C catalyst surface changed from adsorption to dehydrogenation, to hydrolysis and finally oxidation as the electrode potential increased from 0 V to 0.85 V. The main intermediate created during methanol electrochemical oxidation was CO_{ads}. The existence of Sn atoms decreased the onset potential of the hydrolysis reaction, and consequently promoted methanol electrochemical oxidation. Interestingly enough, the highest reaction rate was obtained at about 0.65 V due to similar reaction rates of CO_{ads} oxidation and methanol dehydrogenation.

Manuscript submitted July 13, 2015; revised manuscript received September 17, 2015. Published October 24, 2015.

Direct methanol fuel cells (DMFCs) have been attracting more attention due to fuel abundance, lower cost, safer transformation and storage, and higher volume energy density, compared with other direct alcohol fuel cells (DAFCs).[1–4] However, DMFCs have not been yet utilized at a large scale due to two disadvantages:[2]

(1) Low activity of the anode catalysts. The commonly used Pt/C catalyst can be easily poisoned by the adsorbed intermediates, such as CO_{ads} and -CHO_{ads}, inhibiting the catalytic activity of the Pt/C catalyst for methanol.

(2) Heavy crossover of methanol molecules. The crossover of methanol molecules from the anode to the cathode through the proton exchange membrane not only wastes the fuel, but also creates mixed potential, leading to lower performance.

In recent years, the second problem has been gradually resolved by the development of novel proton exchange membranes,[5–7] however, the first one has not been greatly improved. Developing highly active catalysts for methanol has become the research focus in the DMFCs field.[8–12] At present, the most commonly used DMFCs anode catalysts are Pt and Pt-Ru bimetallic catalysts, which have remarkable theoretical catalytic properties for methanol.[13–15] Generally, Ru element has a bifunctional effect. First, the electron state of Pt atoms can be changed by Ru atoms, leading to reduction of the CO_{ads} adsorption energy. Second, Ru atoms can promote the formation of $(OH)^-_{ads}$, which can react with the CO_{ads} intermediate and generate CO_2, consequently accelerating the methanol electrochemical oxidation process.

Compared with Pt-Ru, the Pt-Sn or Pt-SnO_x catalysts also have remarkable theoretical catalytic properties for methanol, while are less expensive and more abundant. Chu et al., have demonstrated that the PtSn catalysts show similar methanol catalytic activity (i_{PtSn} = 0.57 A, i_{PtRu} = 0.6 A) and higher ethanol catalytic activity (i_{PtSn} = 0.2 A, i_{PtRu} = 0.17 A), compared with the PtRu catalysts.[16] While Neto et al, suggested that the PtSn/C catalyst was more active than the PtRu/C and PtSnRu/C catalysts for methanol and ethanol oxidation at room temperature based on the chronoamperometry experiments results.[17] Thus, the research of the Pt-Sn bimetallic catalyst has attracted more attention in recent years.[18–25] However, the effects of Sn atoms are still unclear, especially whether Sn atoms can promote the formation of $(OH)^-_{ads}$ similar to Ru atoms.

Generally, the development of the new anode catalysts for DMFCs is based on methanol electrochemical oxidation. Unfortunately, regardless of many studies of methanol electrochemical oxidation, the controversy still exists. Particularly, it is still unclear which intermediates will be created during methanol electrochemical oxidation on specific catalysts. It is well-known that the overall electrochemical oxidation of methanol on the Pt-based catalysts is:

$$CH_3OH + H_2O \rightarrow CO_2 + 6H^+ + 6e^- \quad U^0 = 0.046\,V \qquad [1]$$

However, there are many side and transitional reactions during the whole oxidation process, as shown in Figure 1.[26,27] Each reaction step requires one electron transfer, and during methanol oxidation to CO_2, six steps (electrons) are needed, in agreement with Equation 1. The reactions conducted from the left to the right shown in Figure 1 are related to the dehydrogenation of the absorbed methanol molecules and intermediates, while those conducted in the vertical direction are related to the oxidation of the carbon-containing intermediates with the oxygen-containing radicals, usually $(OH)^-_{ads}$.

In summary, methanol electrochemical oxidation on Pt surface includes three main processes.[26] (1) Adsorption of the methanol molecules on the Pt surface. (2) Dehydrogenation of the adsorbed methanol molecules, which will create carbon-containing intermediates. (3) Reactions between the carbon-containing intermediates and oxygen-containing radicals (usually OH^-), which will generate CO_2.

Many methods can be used to study the methanol electrochemical processes conducted in DMFCs, for example in-situ Fourier transform infrared spectroscopy[28,29] and differential electrochemical mass spectrometry, which are suitable to identify the intermediates during the methanol oxidation process.[30] In recent years, electrochemical impedance spectroscopy (EIS) attracts great attention in DMFCs field

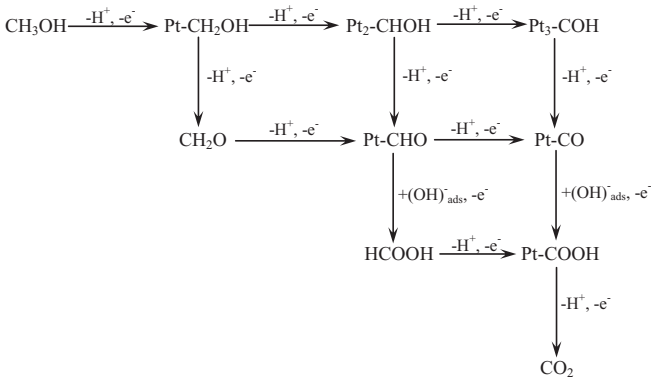

Figure 1. Schematic diagram of methanol electrochemical oxidation on the Pt catalysts. All six reactions along the vertical direction involve the oxygen-containing radical, $(OH)^-_{ads}$. And four of these six reactions were reduced to H^+, based on chemical equilibrium.

[z]E-mail: pangxl@mater.ustb.edu.cn

due to its simplicity and real-time capability.[31] Combing with the theoretical results shown in Figure 1, the methanol oxidation process conducted on the Pt-based catalysts can be easily deduced. It is useful to conduct the study about this issue.

In this paper, methanol electrochemical oxidation on the Pt-SnO_x/C catalyst was studied by cyclic voltammetry (CV) and EIS two simple real-time electrochemical methods, to determine the intermediates created during the reactions and the effects of Sn atoms. Besides, the Sn content effects on the physical and chemical properties of the Pt-SnO_x/C catalysts with different n_{Pt}/n_{Sn} atomic ratios (1:1, 2:1, 3:1, 4:1, 5:1) were studied using energy dispersive spectra (EDS), X-ray diffraction (XRD), transmission electron microscopy (TEM) and X-ray photoelectron spectroscopy (XPS).

Experimental

Catalysts preparation.— The Pt-SnO_x/C catalysts were prepared by the impregnation method, which was conducted as follows. The required amounts of the $H_2PtCl_6 \cdot 6H_2O$ (AR, Pt $\geq$ 37%) and $SnCl_2 \cdot 2H_2O$ (AR, $\geq$98%) precursors, and the Vulcan XC-72R carbon black matrix (Carbot Corp., BET = 250 m^2/g) were added into the isopropanol water solution (1:1) to form homogeneous slurry with ultrasonic dispersion. Then the slurry was heated to 60°C and kept at this temperature for 5 h in the water bath. After that, 1 mol/L NaOH solution was dropped into the slurry to adjust the pH value to 10, and $NaBH_4$ (AR, $\geq$96%) was added into the slurry according to the $n_{Pt}:n_{NaHB4}$ = 1:10 ratio. After 4 h of heating at 60°C, the black solid catalysts were filtered and washed with deionized water until no precipitation was observed by 0.1 mol/L $AgNO_3$ standard solution. Finally the catalysts were dried at 80°C for 12 h in a vacuum oven. Five Pt-SnO_x/C catalysts with different Pt/Sn atomic ratios ($n_{Pt}:n_{Sn}$ = 1:1, 2:1, 3:1, 4:1, 5:1, labeled as Pt_1-SnO_x/C, Pt_2-SnO_x/C, Pt_3-SnO_x/C, Pt_4-SnO_x/C and Pt_5-SnO_x/C, respectively) were prepared, and the nominal loading of Pt in all these catalysts was 20 wt%.

Working electrode preparation.— The glass carbon electrodes (GCEs) with the diameter of 3 mm were used as the working electrode in this research. Before the electrochemical tests, the GCEs were gradually polished by the Al_2O_3 powder (0.1 μm and 0.05 μm), and ultrasonically washed using ethanol, HNO_3 and deionized water solution (1:1) for 1 min, respectively. A mixture containing 2 mg Pt-SnO_x/C catalyst, 200 μl ethanol, 100 μl deionized water and the appropriate amount of 5 wt% Nafion solution (Johnson Matthey Company) was ultrasonically dispersed for 1 h to obtain uniform catalyst ink. 10 μL of this catalyst ink was spread on the GCE surface and dried under an infrared lamp.

Characterization.— The structure of the catalysts was determined using the rotating anode diffractometer (Dmax-RB 12 kW, Rigaku) with the Cu radiation source, λ = 1.5406 Å, and 10–100° 2θ scan range with 10°/min rate. XPS tests were performed on the AXIS ULTRA^{DLD} (SHIMADZU) X-ray photoelectron spectrometer equipped with the Al Kα source, $h\nu$ = 1486.6 eV, and the 12 kV working voltage and the 200 W power. TEM analysis was carried out using the JEOL JEM-2010 electron microscope operated at 200 kV.

The CS350 electrochemical workstation was used to perform the electrochemical measurements in a standard three-electrode system.

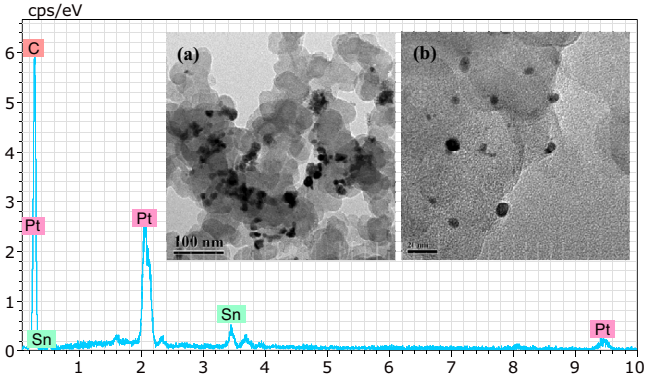

Figure 2. EDS results of the Pt-SnO_x/C catalyst. The insets show the TEM images of the catalysts with different magnification: (a) 40,000×; (b) 100,000×.

The GCE, Pt foil and saturated calomel electrode (SCE) were chosen as the working electrode, the counter-electrode and the reference electrode, respectively. In this paper, all the potentials were recorded with respect to the SCE (vs. SCE).

Two electrochemical methods, CV and EIS, were used to determine the catalytic performance and methanol electrochemical oxidation process. CV experiments were performed in the 0–1.1 V potential range with 20 mV/s scanning speed. EIS experiments were performed between 10^{-2} Hz and 10^5 Hz with 10 points per decade. The amplitude of the sinusoidal potential signal was 5 mV and the electrode potential was set at 0 V, 0.25 V, 0.45 V, 0.65 V and 0.85 V, respectively. Both of these two electrochemical measurements were performed at room temperature in 0.5 mol/L CH_3OH + 0.5 mol/L H_2SO_4 electrolyte solution, which was purged with ultrapure N_2 for 30 min to remove O_2.

Results and Discussion

Morphology and composition.— TEM images in Figure 2 insets show that the catalysts nanoparticles are uniformly dispersed on the surface of the carbon black matrix, and the particle size is about 4–10 nm for all five Pt-SnO_x/C catalysts.

As seen in Figure 2 and Table I, the real loading of the Pt element within these five Pt-SnO_x/C catalysts is about 20 wt%, which is in agreement with the nominal value. The $n_{Pt}:n_{Sn}$ atomic ratio is 1.3, 1.87, 2.88, 4.48 and 5 for the Pt_1-SnO_x/C, Pt_2-SnO_x/C, Pt_3-SnO_x/C, Pt_4-SnO_x/C and Pt_5-SnO_x/C samples, respectively, indicating that the impregnation method used in this research is stable and reliable.

In order to determine the chemical states of the Pt and Sn elements in the catalysts, additional XPS tests were conducted, as shown in Figure 3. For the Pt element, there are two peaks with the binding energy of about 71.7 eV and 75 eV in the Pt4f spectra, which are attributed to the $Pt4f_{7/2}$ and $Pt4f_{5/2}$ energy levels, respectively, as shown in Figure 3a. The Pt4f signal doublet can be fitted with two components, which are ascribed to Pt(0) and Pt(II) two chemical states, respectively. Combined with the EDS and XRD data shown in Structure section, the peaks around 71.7 eV and 75 eV are assigned to metallic Pt, while the peaks around 72.6 eV and 75.59 eV are assigned to

Table I. EDS and XPS results of the Pt-SnO_x/C catalysts.

	EDS					XPS		
Sample	Pt, wt.%	Sn, wt.%	Pt, at.%	Sn, at.%	$n_{Pt}:n_{Sn}$	I_{Pt4f}	I_{Sn3d}	$n_{Pt}:n_{Sn}$
Pt_1-SnO_x/C	18.12	8.54	1.52	1.17	1.3	15640	113250	16:84
Pt_2-SnO_x/C	21.56	7.07	1.81	0.97	1.87	12702	81686	18:82
Pt_3-SnO_x/C	20.14	4.31	1.61	0.56	2.88	14174	45973	30:70
Pt_4-SnO_x/C	23.07	3.15	1.88	0.42	4.48	21466	23925	56:44
Pt_5-SnO_x/C	19.93	2.4	1.55	0.31	5	30922	22527	66:34

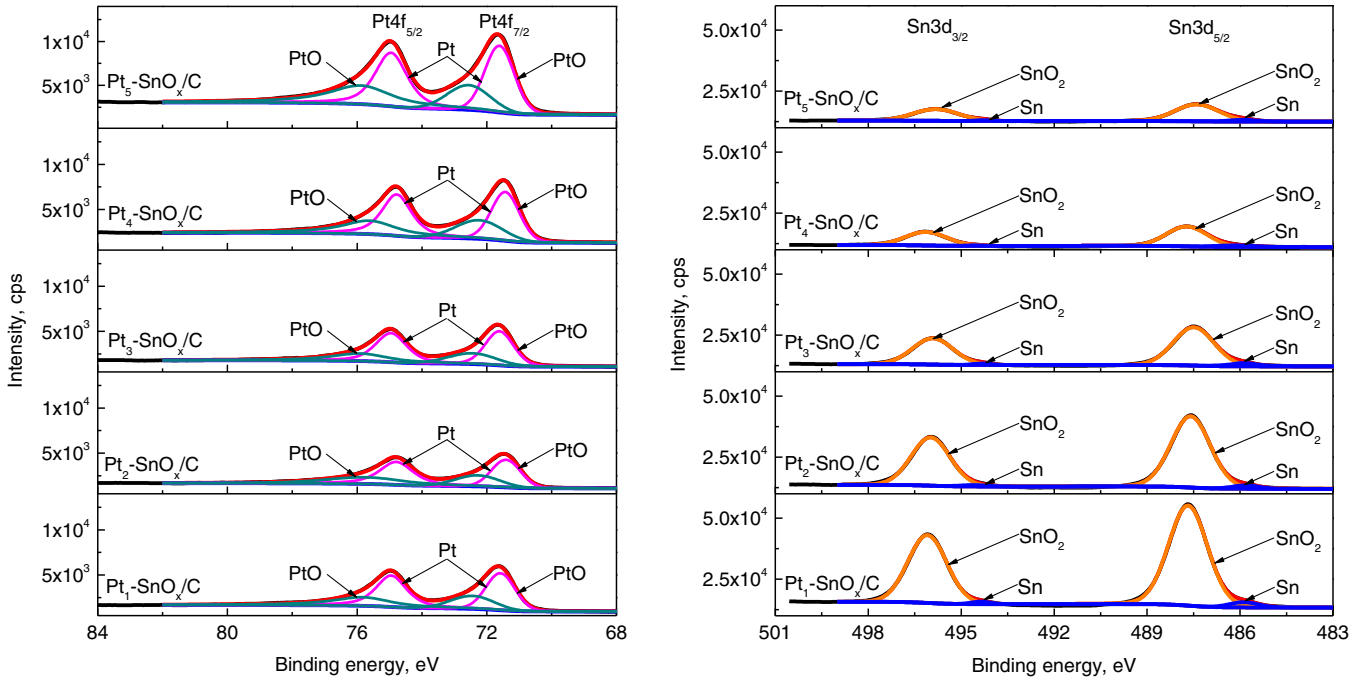

Figure 3. XPS results of the Pt-SnO_x/C catalysts with different Pt/Sn ratios: (a) Pt4f; (b) Sn3d.

PtO. The existence of PtO in the catalysts is attributed to the long air exposure. Nevertheless, Pt is the major component in all samples according to the area of the peaks.

For the Sn element, there are also two peaks with the binding energy of 487.5 eV and 495.9 eV in the Sn3d spectra, corresponding to $Sn3d_{5/2}$ and $Sn3d_{3/2}$ energy levels, respectively, as shown in Figure 3b. The Sn3d signal doublet can be fitted with two components, which are ascribed to Sn(0) and Sn(IV) two chemical states, respectively. Combined with the EDS and XRD results shown in Structure section, the peaks around 485.9 eV and 494.3 eV are assigned to metallic Sn, and the peaks around 487.7 eV and 496.1 eV are assigned to SnO_2. Hence, for the SnO_x, x equals 0 and 2 based on the above results. Particularly, the content of SnO_2 is much higher than the Sn chemical state due to long air exposure. However, the Sn oxides can provide oxygen-containing species for oxidizing intermediates (e.g. CO_{ads}) chemisorbed on the adjacent active Pt sites, which consequently promotes the methanol electrochemical oxidation.[32]

The relative content of the Pt and Sn elements on the catalyst surface was calculated using the relative sensitivity factors (RSFs) method:[33]

$$\frac{n_i}{n_j} = \frac{I_i / S_i}{I_j / S_j} \qquad [2]$$

where n_i/n_j represents the atomic ratio between the element i and j, I_i and I_j denote the peak area, while S_i and S_j are the RSFs of the two elements. In the present work, the RSFs of the Pt4f and Sn3d are 5.575 and 7.875, respectively, and the quantified results are listed in Table I. Apparently, the atomic ratios of the Pt and Sn elements on the catalysts surface change with the Sn content in the solution. Besides, the Sn content on the catalyst surface is much higher than the nominal value, indicating that the Sn atoms tend to accumulate on the catalyst surface. This may inhibit the growth of the Pt-SnO_x particles confirmed by the XRD results shown below.

Structure.— Figure 4 shows XRD patterns of the Pt-SnO_x/C catalysts. The intensity peaks at 39°, 46°, 67°, 81° and 85° are attributed to Pt(111), Pt(200), Pt(200), Pt(311) and Pt(222), respectively, indicating typical face centered cubic (fcc) structure. The positions of all the Pt diffraction peaks are slightly shifted toward larger 2θ values as

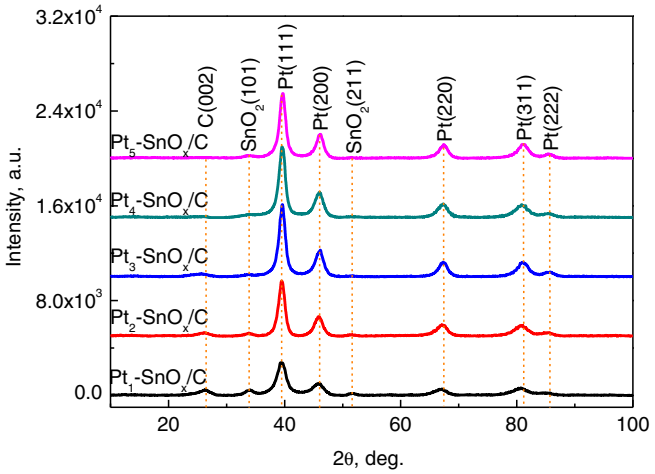

Figure 4. XRD patterns of the Pt-SnO_x/C catalysts with different Pt/Sn ratios.

the Sn content decreases, which may be attributed to the formation of the PtSn binary alloy. Moreover, the width of the Pt diffraction peaks gradually becomes lager as the Sn content increases, indicating that the lattice parameters of the Pt crystal increase with the Sn content, as listed in Table II.

The peaks at about 26°, 34° and 52° are attributed to C(110), SnO_2(101) and SnO_2(211), respectively.[34] It is interesting to note that the intensity of the SnO_2(101) peak increases with the Sn contents,

Table II. Structure parameters of the Pt-SnO_x/C catalysts.

Sample	Position of Pt(220)	Particle Size, nm	Lattice constant, Å
Pt_1-SnO_x/C	67.16°	3.8	3.94
Pt_2-SnO_x/C	67.16°	4.4	3.938
Pt_3-SnO_x/C	67.28°	5.1	3.933
Pt_4-SnO_x/C	67.4°	5.4	3.932
Pt_5-SnO_x/C	67.4°	5.8	3.926

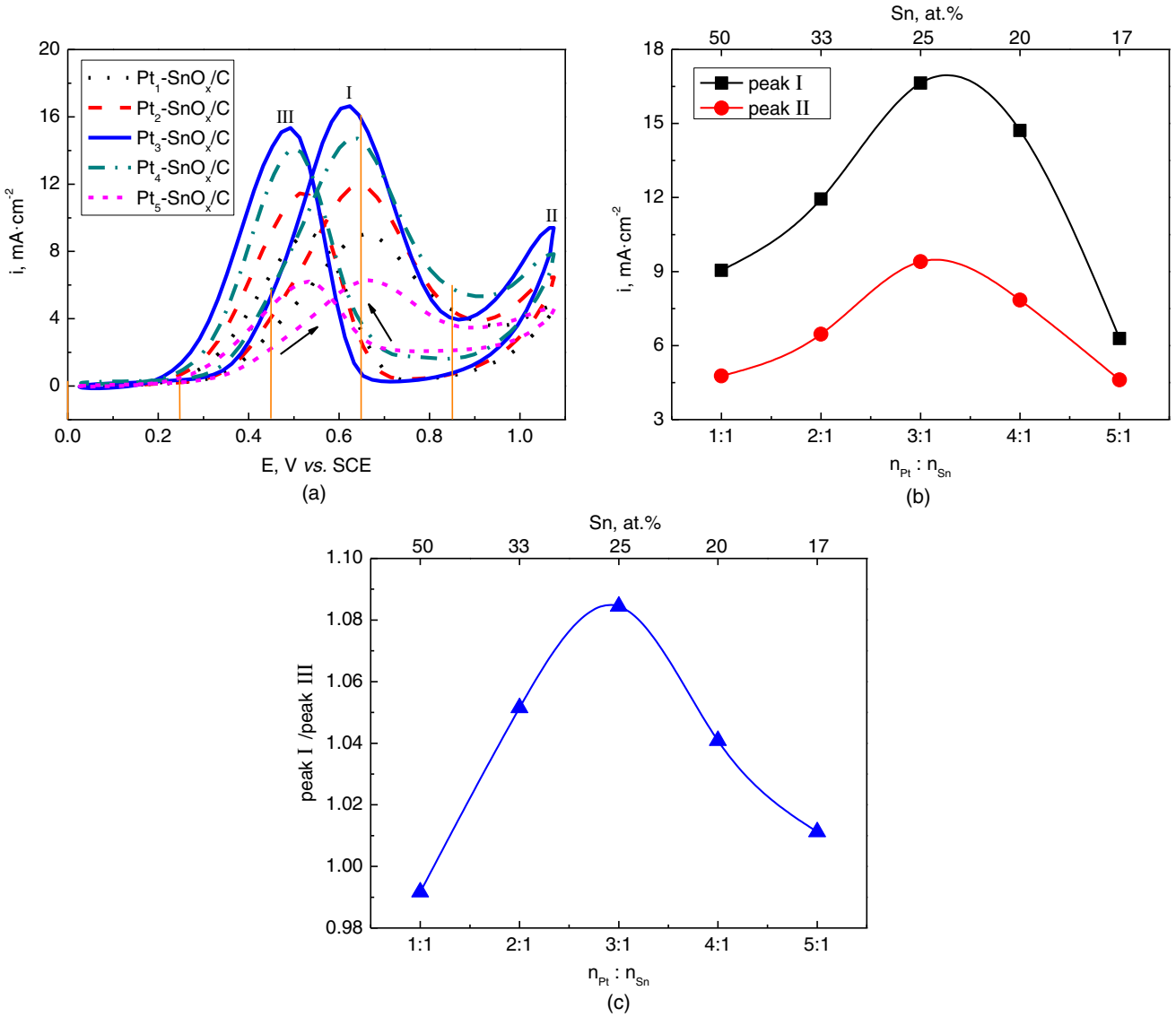

Figure 5. (a) Cyclic voltammograms of the Pt-SnO_x/C catalysts obtained in the 0.5 mol/L CH_3OH+0.5 mol/L H_2SO_4 solution with 20 mV/s scanning rate; (b) intensity of the oxidation peak I and II as a function of the composition of the Pt-SnO_x/C catalysts; (c) ratio of the peak I and peak III intensities as a function of the composition of the Pt-SnO_x/C catalysts.

indicating that more Sn crystalline exists with the higher Sn content in the catalysts. It is necessary to note that there are no diffraction peaks belonging to PtO and Sn, which is inconsistent with the XPS results. This may be attributed to the poor crystallinity and relatively small amounts of these two phases in the Pt-SnO_x/C catalysts.

The average particle size of the Pt-SnO_x/C catalysts was estimated by the Debye-Scherrer formula:[35]

$$d = \frac{0.9\lambda}{\beta \cos\theta} \qquad [3]$$

where d denotes the average particle size, the value 0.9 comes from the spherical crystallite geometry, λ is the wavelength of X-ray radiation (Cu, Kα, $\lambda = 1.5406$ Å), β represents the full width at half maximum (FWHM) of the Pt(220) peak and θ is the diffraction angle corresponding to the Pt(220) peak maximum. Selecting the Pt(220) reflection can eliminate the influences of the carbon matrix and Sn diffraction peaks. As seen in Table II, the average particle size of the Pt-SnO_x/C catalysts ranges from 3.8 nm to 5.4 nm, which is in agreement with the TEM results. Moreover, the average particle size decreases as the Sn content increases, which is attributed to the SnO_2 phase accumulates on the catalysts surface and inhibits the Pt particle growth.[36]

Catalytic properties.— Cyclic voltammetry was used to estimate the catalytic properties of the Pt-SnO_x/C catalysts for methanol within this research. The cyclic voltammograms were obtained in 0–1.1 V potential range with 20 mV/s scanning speed, as shown in Figure 5a. Three peaks labeled as I, II and III were obtained within the whole scanning potential range, which are related to the methanol electrochemical oxidation, water electrolysis and intermediates electrochemical reduction reactions, respectively. Moreover, the onset potentials of the methanol oxidation for these five Pt-SnO_x/C catalysts are similar, about 0.2 V, which is close to the value obtained on pure Pt catalysts.[37]

As the Sn content in the catalysts decreases, the maximum current densities of the methanol electrochemical oxidation and the water electrolysis reaction increase to a maximum and then decrease, as seen in Figure 5b. The Pt_3-SnO_x/C catalyst shows the highest values of about 16.6 mA/cm^2 (peak I) and 15.3 mA/cm^2 (peak II), respectively, which are much larger than the Pt/C catalysts[38] and close to the Pt-Ru/C catalysts.[39,40] This indicates that the Pt-SnO_x/C catalyst is a potential substitute for the Pt-Ru/C catalysts. These variations can be

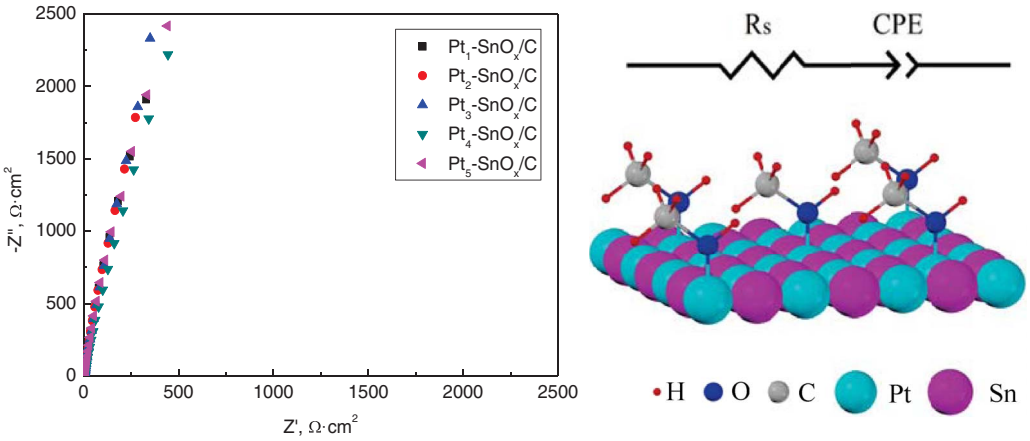

Figure 6. Nyquist plots of the Pt-SnO_x/C catalysts obtained at 0 V in 0.5 mol/L CH_3OH + 0.5 mol/L H_2SO_4 solution. In the equivalent circuit, R_s and CPE represent the solution resistance and the constant phase angle element, respectively. The schematic diagram shows the adsorption of the methanol molecules on the Pt-SnO_x/C catalysts surface.

explained by the dual effects of Sn atoms mentioned above. When the Sn content in the catalysts is low enough, the Pt d band of the PtSn particles was narrower and was shifted down relative to the Fermi level when increasing the Sn content, leading to lower CO_{ads} adsorption over the bimetallic system than the monometallic system.[41] Moreover, it is easier to create $(OH)_{ads}$ on Sn atoms, compared with Pt atoms, which can promote methanol electrochemical oxidation. However, as shown in Table II, the lattice constant values of the Pt-SnO_x/C catalysts increase almost linearly with the Sn content. Besides, all these values are larger than the lattice constant value of pure Pt (3.924 Å), indicating that the Sn atoms may exist in the Pt lattice and create crystal defects. Hence, too high Sn content in the catalysts may damage the integrity of the Pt lattice and hinder the adsorption of methanol on the Pt surface, therefore degrading the catalyst performance.[25] There is an optimal Sn content in the Pt-SnO_x/C catalysts, and 3:1 (Sn 25 wt%) is the optimal n_{Pt}:n_{Sn} value within this research.

Besides, there is also an optimal relation between the average particle size and the catalytic properties of the catalysts. The small particle size may lead to high surface activity of the catalyst particles, and consequently promote CO_{ads} adsorption, which can degrade the catalysts performance. Large particle size may leads to low active centers of the catalysts, which can also degrade the catalytic properties. The optimal average particle size is about 5 nm within this research.

Generally, the ratio of the maximum current density of the peaks I and II can be used to describe the catalyst tolerance to intermediate species accumulation.[42] The higher ratio indicates better electrochemical oxidation of methanol to CO_2 during the forward scan, i.e., less intermediates are left. The ratios for the Pt_1-SnO_x/C, Pt_2-SnO_x/C, Pt_3-SnO_x/C, Pt_4-SnO_x/C and Pt_5-SnO_x/C catalysts are 0.99, 1.05, 1.08, 1.04 and 1.01, respectively, as seen in Figure 5c. Obviously, the Pt_3-SnO_x/C catalyst shows highest catalytic properties, compared with the other four Pt-SnO_x/C catalysts.

Methanol electrochemical oxidation mechanism.— EIS was used to study the electrochemical oxidation process of methanol on the Pt-SnO_x/C catalysts. According to the Nyquist plot results, especially the corresponding equivalent circuits, one can deduce the possible reaction process conducted on the catalyst surface. Within this research, five typical DC potentials (0 V, 0.25 V, 0.45 V, 0.65 V and 0.85 V), corresponding to different reaction processes were chosen for the EIS tests based on Figure 5a.

The main reaction conducted on the Pt-SnO_x/C surface is the chemi-adsorption of the methanol molecules at 0 V potential, according to the linear Nyquist plots and their equivalent circuit in Figure 6. Moreover, the equivalent circuit is composed of two elements in series, the solution resistance (R_s) between the working electrode and the reference electrode, and the constant phase angle element (CPE), representing the double layer capacitance of the absorbed methanol. According to the previous research, the main methanol absorption sites are Pt atoms instead of the Sn atoms due to the difference in electronic structure.[43] The principal bonding orbital of methanol on the Pt surface belongs to the oxygen atom, which has one lone pair of electrons, as shown in Figure 6. Besides, the plots of these five Pt-SnO_x/C catalysts are quite similar to each other confirmed by the fitting parameters shown in Table III. This indicates that methanol adsorption is hardly affected by the composition of the Pt-SnO_x/C catalysts at this potential.

When the potential increases to 0.25 V, the Nyquist plots of the Pt-SnO_x/C catalysts show a large capacitive reactance arc in the high and middle frequency range and a pseudo-inductive arc in the low frequency range, as shown in Figure 7. It is worth to note that Pt_3-SnO_x/C has the smallest capacitive reactance arc radius, i.e., the smallest charge transfer resistance (R_t) shown in Table IV. This indicates that the electrochemical oxidation conducted on the Pt_3-SnO_x/C surface has the highest rate compared with the other four Pt-SnO_x/C catalysts, which is in agreement with the CV results. According to the equivalent circuit shown in Figure 7, there are two different time constants, the capacitance (C_1 and C_2) and the inductance (L), related to the methanol dehydrogenation and the intermediates adsorption reactions (especially CO_{ads}) shown in Figure 7. The reaction rate of the five Pt-SnO_x/C catalysts is different from each other according to the fitting parameters (R_1, R_2 and R_3) in Table IV. This trend is inconsistent with the CV results, which may be attributed to the difficulty of reaching steady state at this potential. Moreover, the pseudo-inductive arcs of the Nyquist plots shown in the fourth quadrant are attributed to the strong CO_{ads} adsorption on the Pt sites compared with the carbon-containing intermediates. This can inhibit methanol electrochemical oxidation into CO_2.[44] The catalyst surface coverage responds slowly to the alternating electrode potential due to the strong adsorption of CO_{ads}, leading to a delay between the potential perturbation and the resulting alternating current, i.e. a pseudo-inductance in the Nyquist plots.

Table III. Fitting parameters based on the equivalent circuit shown in Fig. 6.

Sample	R_s, Ω · cm²	CPE, ×10⁻³ F · cm⁻²
Pt_1-SnO_x/C	1.266	7.093
Pt_2-SnO_x/C	1.694	7.229
Pt_3-SnO_x/C	1.413	5.601
Pt_4-SnO_x/C	1.227	5.661
Pt_5-SnO_x/C	1.527	5.297

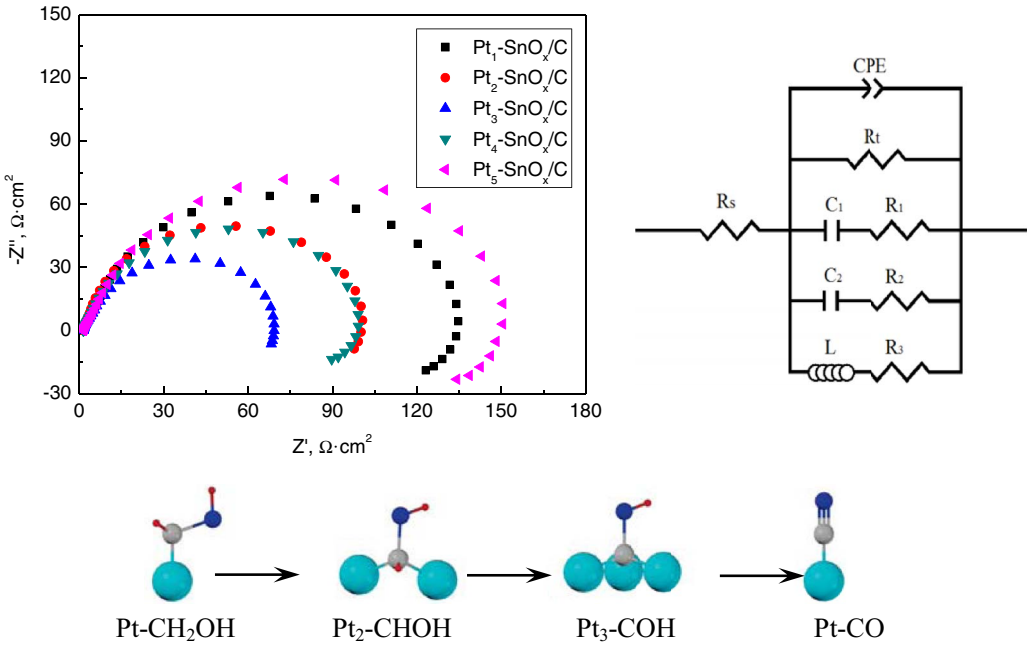

Figure 7. Nyquist plots of the Pt-SnO_x/C catalysts obtained at 0.25 V in 0.5 mol/L CH_3OH + 0.5 mol/L H_2SO_4 solution. In the equivalent circuit, R_s, CPE and R_t represent the solution resistance, the constant phase angle element and the charge transfer resistance of the whole system, respectively; C_1 (C_2) and L represent the capacitance and the inductance component of the methanol dehydrogenation and the intermediates adsorption, respectively; R_1, R_2 and R_3 represent the charge transfer resistance corresponding to the three steps of the dehydrogenation reactions conducted on the Pt-SnO_x/C catalysts surface. The schematic diagram shows the dehydrogenation reactions of the methanol molecules conducted on the Pt-SnO_x/C catalysts surface.

The radius of the pseudo-inductive arc increases as the potential increases to 0.45 V, as seen in Figure 8. Apparently, Pt_3-SnO_x/C still has the smallest capacitive reactance arc radius confirmed by the R_t value in Table V, indicating the fastest electrochemical oxidation of the methanol on the Pt_3-SnO_x/C surface. According to the equivalent circuit in Figure 8, there are two inductance components, L_1 and L_2, which may be related to the adsorption of CO_{ads} and $(OH)^-_{ads}$, deduced from methanol electrochemical oxidation on pure Pt catalysts.[27] Generally, the favored adsorption sites for $(OH)^-_{ads}$ are Sn atoms, instead of Pt atoms based on the difference of the adsorption energy on these two sites.[43] Moreover, the R_{t1} value for the electrochemical oxidation of CO_{ads} is much larger than R_{t2}, which is related to the hydrolysis reaction, as listed in Table V. Hence, combined with the CV results, it's interesting to note that the existence of Sn atoms in the Pt catalysts can decrease the onset potential of the hydrolysis reaction, and consequently promote CO_{ads} electrochemical oxidation.[45]

As the potential increases to 0.65 V, the Nyquist plots flip to the second quadrant in the high and middle frequency range, as shown in Figure 9. This indicates that the rate determining step of the electrochemical oxidation changed from the CO_{ads} oxidation to the methanol dehydrogenation.[46] The rates of these two reactions will approach each other with the increasing potential. When the potential is high enough, the rate of the CO_{ads} oxidation will exceed that of the methanol dehydrogenation, confirmed by the R_{t1} and R_{t2} values in Table VI, leading to the abrupt flip of the Nyquist plots to the second quadrants. It is interesting to note that the Nyquist plots contain a large capacitive reactance arc in the low frequency range, which is related to the electrochemical oxidation on the Pt-SnO_x/C surface. Apparently, Pt_3-SnO_x/C still has the smallest radius compared with the other four catalysts confirmed by the R_t values in Table VI. Based on the equivalent circuit, the competition between these two reactions leads to the relaxation of the electrochemical oxidation process, which is represented by the inductance component L in Figure 9.

When the potential reaches 0.85 V, the Nyquist plots shows a large capacitive reactance arc in the high and middle frequency range, and a small diffusion impedance arc (Warburg impedance) in the low frequency range, as shown in Figure 10. This indicates that the rate determining step may be the diffusion of the reactants at high potential. According to the equivalent circuit in Figure 10, the finite diffusion impedance (Z_W) is attributed to the diffusion of the methanol molecules to the Pt-SnO_x/C catalysts surface, and the fitting values of Z_W are similar, as listed in Table VII, indicating that the diffusion process is similar for these five Pt-SnO_x/C catalysts at high potential. In addition, the radius of the capacitive reactance arc (R_t) for Pt_3-SnO_x/C is much smaller than the other four Pt-SnO_x/C catalysts, indicating easier oxidation of methanol on the Pt_3-SnO_x/C catalysts.

In summary, methanol electrochemical oxidation reaction conducted on the Pt-SnO_x/C catalysts undergoes adsorption, dehydrogenation, hydrolysis and oxidation as the electrode potential increases from 0 V to 0.85 V. At 0.65 V the rates of CO_{ads} oxidation and the methanol dehydrogenation are similar. Sn atoms in the Pt catalysts can decrease the onset potential of the hydrolysis reaction, and consequently promote CO_{ads} electrochemical oxidation.

Table IV. Fitting parameters based on the equivalent circuit shown in Fig. 7.

Sample	R_s, $\Omega \cdot cm^2$	CPE, $\times 10^{-3}$ $F \cdot cm^{-2}$	R_t, $\Omega \cdot cm^2$	C_1, $\times 10^{-3}$ $F \cdot cm^{-2}$	R_1, $\Omega \cdot cm^2$	C_2, $\times 10^{-3}$ $F \cdot cm^{-2}$	R_2, $\Omega \cdot cm^2$	L, $H \cdot cm^2$	R_3, $\Omega \cdot cm^2$
Pt_1-SnO_x/C	1.287	2.074	137.2	1.811	2.729	2.002	28.84	6387	205.3
Pt_2-SnO_x/C	1.389	6.253	101.5	5.324	1.824	3.091	12.89	6451	174.8
Pt_3-SnO_x/C	1.441	7.339	70.04	2.085	6.229	6.212	19.62	4494	102
Pt_4-SnO_x/C	1.571	3.301	100.2	2.696	3.158	1.553	23.75	4614	168.1
Pt_5-SnO_x/C	1.526	1.772	155.8	1.824	2.675	1.887	27.34	5917	237.5

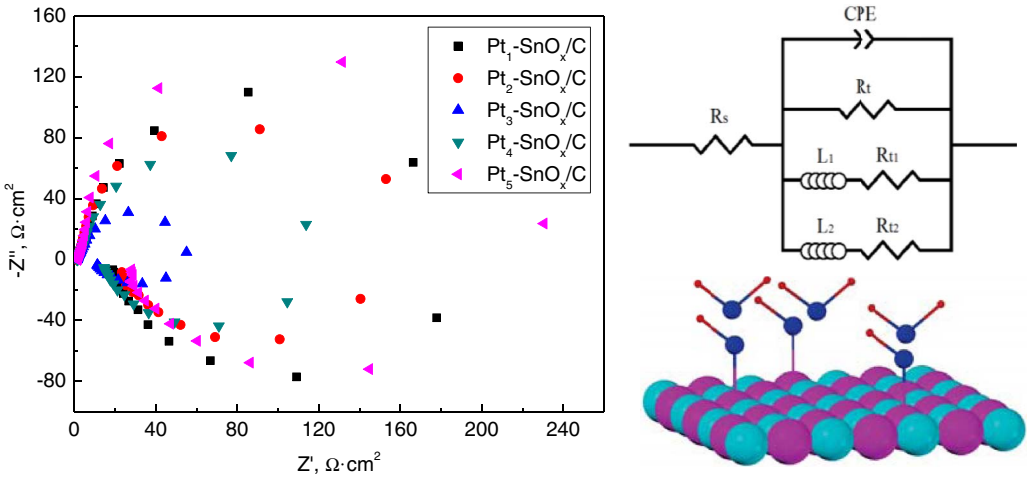

Figure 8. Nyquist plots of the Pt-SnO_x/C catalysts obtained at 0.45 V in 0.5 mol/L CH_3OH + 0.5 mol/L H_2SO_4 solution. In the equivalent circuit, R_s, CPE and R_t represent the solution resistance, the constant phase angle element and the charge transfer resistance of the whole system, respectively; L_1 (L_2) and R_{t1} (R_{t2}) represent the inductive impedance and the charge transfer resistance of the adsorption reaction of CO_{ads} and $(OH)^-_{ads}$ proceeding on the Pt-SnO_x/C catalysts surface, respectively. The schematic diagram shows the generation of $(OH)^-_{ads}$ on Sn atoms.

Table V. Fitting parameters based on the equivalent circuit shown in Fig. 8.

Sample	R_s, $\Omega \cdot cm^2$	CPE, $\times 10^{-3}$ $F \cdot cm^{-2}$	R_t, $\Omega \cdot cm^2$	L_1, $H \cdot cm^2$	R_{t1}, $\Omega \cdot cm^2$	L_2, $H \cdot cm^2$	R_{t2}, $\Omega \cdot cm^2$
Pt_1-SnO_x/C	1.204	7.166	199.3	123.1	173.54	162.7	32.31
Pt_2-SnO_x/C	1.179	7.948	183.2	103.2	126.03	391.8	28.45
Pt_3-SnO_x/C	1.254	7.211	52.79	35.02	145.65	111.1	15.13
Pt_4-SnO_x/C	1.47	9.455	115.5	109.7	115.79	69.67	26.57
Pt_5-SnO_x/C	1.594	7.446	244.1	351.6	151.41	102.7	47.93

Conclusions

Five Pt-SnO_x/C catalysts with different Pt/Sn atomic ratios (1:1, 2:1, 3:1, 4:1 and 5:1) were successfully prepared by the impregnation method. The composition of the Pt-SnO_x/C catalysts was in agreement with the designed value, and the average particle size increased from 3.8 nm to 5.4 nm as the Sn content decreased, confirmed by the TEM and XRD results. There are two chemical states (Pt and PtO, Sn and SnO_2) for Pt and Sn elements existing in the catalysts, respectively. The content of the chemical states of Pt and PtO is almost equal, while

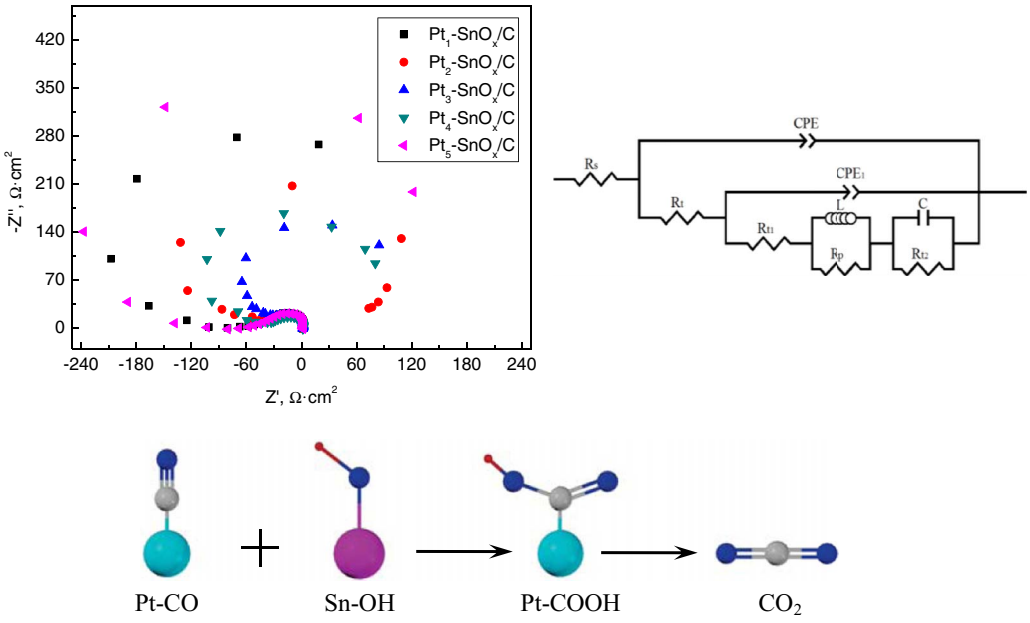

Figure 9. Nyquist plots of the Pt-SnO_x/C catalysts obtained at 0.65 V in 0.5 mol/L CH_3OH + 0.5 mol/L H_2SO_4 solution. In the equivalent circuit, R_s, CPE and R_t represent the solution resistance, the constant phase angle element and the charge transfer resistance of the whole system, respectively; CPE_1 and R_{t1} represent the constant phase angle element and charge transfer resistance corresponding to the oxidation of CO_{ads} to CO_2, respectively; L, R_p, C and R_{t2} represent the inductive impedance, the polarization resistance, the capacitance and the charge transfer resistance corresponding to the methanol dehydrogenation reactions. The schematic diagram shows electrochemical oxidation of CO_{ads} into CO_2.

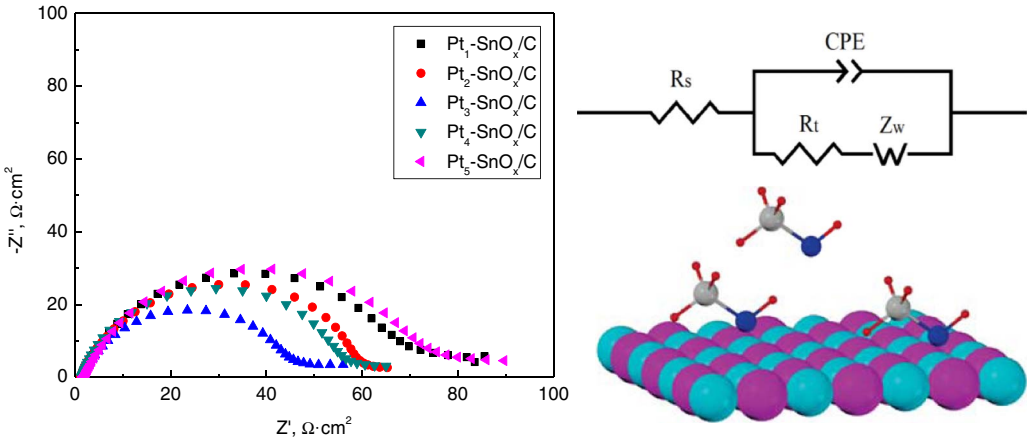

Figure 10. Nyquist plots of the Pt-SnO_x/C catalysts obtained at 0.85 V in 0.5 mol/L CH_3OH + 0.5 mol/L H_2SO_4 solution. In the equivalent circuit, R_s, CPE and R_t represent the solution resistance, the constant phase angle element and the charge transfer resistance of the whole system, respectively; Z_W represents the finite diffusion impedance (Warburg impedance) corresponding to the diffusion of the methanol molecules from the solution to the Pt-SnO_x/C catalyst surface. The schematic diagram shows the diffusion of the methanol molecules from the solution to the Pt-SnO_x/C catalyst surface.

Table VI. Fitting parameters based on the equivalent circuit shown in Fig. 9.

Sample	R_s, $\Omega \cdot cm^2$	CPE, $\times 10^{-3}$ $F \cdot cm^{-2}$	R_t, $\Omega \cdot cm^2$	CPE_1, $\times 10^{-3}$ $F \cdot cm^{-2}$	R_{t1}, $\Omega \cdot cm^2$	L, $H \cdot cm^2$	R_p, $\Omega \cdot cm^2$	C, $\times 10^{-3}$ $F \cdot cm^{-2}$	R_{t2}, $\Omega \cdot cm^2$
Pt_1-SnO_x/C	1.424	2.846	43.62	2.531	268.51	59.55	21.41	4.164	51.47
Pt_2-SnO_x/C	1.362	3.076	40.68	9.467	204.7	56.48	17.28	1.773	49.41
Pt_3-SnO_x/C	1.422	6.177	30.77	2.421	100.1	20.94	17.41	6.386	34.16
Pt_4-SnO_x/C	1.555	2.604	39.31	5.077	120.3	15.18	25.87	2.877	48.12
Pt_5-SnO_x/C	1.286	2.772	49.97	7.352	299.8	88.71	11.42	1.152	66.84

Note: the absolute values are shown.

the content of SnO_2 is much higher than the Sn chemical state due to the long air exposure. According to the CV results, when the Sn content in the catalysts decreases, the maximum current density of the electrochemical oxidation of methanol increases to a maximum first and then decreases. The Pt_3-SnO_x/C catalyst shows the highest value of about 16.6 $mA \cdot cm^{-2}$.

Methanol electrochemical oxidation on the Pt-SnO_x/C catalysts was studied by the simple real-time EIS method. The process progressed from adsorption to dehydrogenation, to hydrolysis and finally oxidation as the electrode potential increased from 0 V to 0.85 V, based on the Nyquist plots and the simulated equivalent circuit. The main intermediates during the electrochemical oxidation of methanol on the Pt-SnO_x/C catalysts is CO_{ads}. It was generated at the potential of about 0.25 V, and the existence of Sn atoms decreased the onset potential of the hydrolysis reaction and promoted the $(OH)^-_{ads}$ creation. The highest reaction rate was obtained at about 0.65 V due to similar reaction rates of CO_{ads} oxidation and methanol dehydrogenation.

Acknowledgments

This work was supported by the National Nature Science Foundation of China (51271022), the Fok Ying Tung Education Foundation (132001) and the Fundamental Research Funds for the Central Universities (FRF-TP-14-008A2). Alex Volinsky acknowledges support from the National Science Foundation under the IRES 1358088 grant.

Table VII. Fitting parameters based on the equivalent circuit shown in Fig. 10.

Sample	R_s, $\Omega \cdot cm^2$	CPE, $\times 10^{-3}$ $F \cdot cm^{-2}$	R_t, $\Omega \cdot cm^2$	Z_W, $\Omega \cdot cm^2$
Pt_1-SnO_x/C	1.676	7.203	73.63	1.473
Pt_2-SnO_x/C	1.209	6.372	61.61	1.875
Pt_3-SnO_x/C	1.405	8.843	47.73	2.647
Pt_4-SnO_x/C	1.427	7.878	58.15	1.915
Pt_5-SnO_x/C	1.817	6.223	79.41	2.65

References

1. W. Vielstich, A. Lamm, and H. A. Gasteiger. Handbook of Fuel Cells: Fundamentals, Technology, Applications. 2003.
2. R. O'Hayre, S. W. Cha, W. Colella, and F. B. Prinz. *Fuel Cell Foundanmentals.* 2009.
3. K. Wippermann, R. Elze, C. Wannek, H. Echsler, and D. Stolten, "Influence of the ionomer type in direct methanol fuel cell (DMFC) anode catalyst layers on the properties of primary and secondary pores," *J. Power Sources*, **228**, 57 (2013).
4. M. Y. Lo, I. H. Liao, and C. C. Huang, "Key issues in the preparation of DMFC electrocatalysts," *Int. J. Hydrogen Energ.*, **32**, 731 (2007).
5. C. J. Zhao, H. D. Lin, and H. Na, "Novel cross-linked sulfonated poly (arylene ether ketone) membranes for direct methanol fuel cell," *Int. J. Hydrogen Energ.*, **35**, 2176 (2010).
6. Y. H. Seong, J. Won, S. K. Kim, K. Nam, S. K. Kim, and D. W. Kim, "Synthesis and characterization of proton exchange membranes based on sulfonated poly (fluorenyl ether nitrile oxynaphthalate) for direct methanol fuel cells," *Int. J. Hydrogen Energ.*, **36**, 8492 (2011).
7. T. Nguyen and X. Wang, "Multifunctional composite membrane based on a highly porous polyimide matrix for direct methanol fuel cells," *J. Power Sources*, **195**, 1024 (2010).
8. H. J. Chun, D. B. Kim, D. H. Lim, W. D. Lee, and H. I. Lee, "A synthesis of CO-tolerant Nb_2O_5-promoted Pt/C catalyst for direct methanol fuel cell: its physical and electrochemical characterization," *Int. J. Hydrogen Energ.*, **35**, 6399 (2010).
9. S. Basri, S. K. Kamarudin, W. R. W. Daud, and Z. Yaakub, "Nanocatalyst for direct methanol fuel cell (DMFC)," *Int. J. Hydrogen Energ.*, **35**, 7957 (2010).
10. B. Piela, T. S. Olson, P. Atanassov, and P. Zelenay, "Highly methanol-tolerant non-precious metal cathode catalysts for direct methanol fuel cell," *Electrochim. Acta*, **55**, 7615 (2010).
11. E. A. Franceschini, M. M. Bruno, F. A. Viva, F. J. Williams, M. Jobbágy, and H. R. Corti, "Mesoporous Pt electrocatalyst for methanol tolerant cathodes of DMFC," *Electrochim. Acta*, **71**, 173 (2012).
12. K. T. Jeng, N. Y. Hsu, and C. C. Chien, "Synthesis and evaluation of carbon nanotube-supported RuSe catalyst for direct methanol fuel cell cathode," *Int. J. Hydrogen Energ.*, **36**, 3997 (2011).

13. N. Tsiouvaras, M. V. Martínez-Huerta, O. Paschos, U. Stimming, J. L. G. Fierro, and M. A. Peña, "PtRuMo/C catalysts for direct methanol fuel cells: Effect of the pretreatment on the structural characteristics and methanol electrooxidation," *Int. J. Hydrogen Energ.*, **35**, 11478 (2010).
14. S. H. Lee, N. Kakati, S. H. Jee, J. Maiti, and Y. S. Yoon, "Hydrothermal synthesis of PtRu nanoparticles supported on graphene sheets for methanol oxidation in direct methanol fuel cell," *Mater. Lett.*, **65**, 3281 (2011).
15. O. Sahin and H. Kivrak, "A comparative study of electrochemical methods on Pt-Ru DMFC anode catalysts: the effect of Ru addition," *Int. J. Hydrogen Energ.*, **38**, 901 (2013).
16. Y. H. Chu and Y. G. Shul, "Combinatorial investigation of Pt-Ru-Sn alloys as an anode electrocatalysts for direct alcohol fuel cells," *Int. J. Hydrogen Energ.*, **35**, 11261 (2010).
17. A. O. Neto, R. R. Dias, M. M. Tusi, M. Linardi, and E. V. Spinacé, "Electro-oxidation of methanol and ethanol using PtRu/C, PtSn/C and PtSnRu/C electrocatalysts prepared by an alcohol-reduction process," *J. Power Sources*, **166**, 87 (2007).
18. B. J. Su, K. W. Wang, T. C. Cheng, and C. J. Tseng, "Preparation of PtSn/C electrocatalysts with improved activity and durability toward oxygen reduction reaction by alcohol-reduction process," *Mater. Chem. Phys.*, **135**, 395 (2012).
19. J. R. Martínez, A. S. Escribano, J. A. Anderson, and F. R. Reinoso, "Influence of the preparation method on the catalytic behavior of PtSn/TiO_2 catalysts," *Catal. Today*, **123**, 235 (2007).
20. K. Nam, S. Lim, S. K. Kim, S. H. Yoon, and D. H. Jung, "Application of silica as a catalyst support at high concentrations of methanol for direct methanol fuel cells," *Int. J. Hydrogen Energ.*, **37**, 4619 (2012).
21. M. Y. Zhu, G. Q. Sun, and Q. Xin, "Effect of alloying degree in PtSn catalyst on the catalytic behavior for ethanol electro-oxidation," *Electrochim. Acta*, **54**, 1511 (2009).
22. J. H. Kim, S. M. Choi, S. H. Nam, M. H. Seo, S. H. Choi, and W. B. Kim, "Influence of Sn content on PtSn/C catalysts for electrooxidation of C1-C3 alcohols: Synthesis, characterization, and electrocatalytic activity," *Appl. Catal. B: Environ.*, **82**, 89 (2008).
23. S. S. Gupta, S. Singh, and J. Datta, "Promoting role of unalloyed Sn in PtSn binary catalysts for ethanol electro-oxidation," *Mater. Chem. Phys.*, **116**, 223 (2009).
24. E. A. Baranova, M. A. Padilla, B. Halevi, T. Amir, K. Artyushkova, and P. Atanassov, "Electrooxidation of ethanol on PtSn nanoparticles in alkaline solution: correlation between structure and catalytic properties," *Electrochim. Acta*, **80**, 377 (2012).
25. S. G. Rodríguez, F. Somodi, I. Borbáth, J. L. Margitfalvi, M. A. Peña, J. L. G. Fierro, and S. Rojas, "Controlled synthesis of Pt-Sn/C fuel cell catalysts with exclusive Sn-Pt interaction application in CO and ethanol electrooxidation reactions," *Appl. Catal. B: Environ.*, **91**, 83 (2009).
26. L. Carrette, K. A. Friedrich, and U. Stimming, "Fuel cells fundamentals and applications," *Fuel Cell*, **1**, 5 (2001).
27. A. Hamnett, "Mechanism and electrocatalysis in the direct methanol fuel cell," *Catal. Today*, **38**, 445 (1997).
28. D. Liu, G. H. Que, Z. X. Wang, and Z. F. Yan, "In situ FT-IR study of CO and H_2 adsorption on a Pt/Al_2O_3 catalyst," *Catal. Today*, **68**, 155 (2001).
29. Y. Morimoto and E. B. Yeager, "Comparison of methanol oxidations on Pt, Pt|Ru and Pt|Sn electrodes," *J. Electroanal. Chem.*, **444**, 95 (1998).
30. T. Seiler, E. R. Savinova, K. A. Friedrich, and U. Stimming, "Poisoning of PtRu/C catalysts in the anode of a direct methanol fuel cell: a DEMS study," *Electrochim. Acta*, **49** 3927 (2004).
31. S. Wasmus and A. Küver, "Methanol oxidation and direct methanol fuel cells: a selective review," *J. Electroanal. Chem.*, **461**, 14 (1996).
32. T. E. Shubina and M. T. M. Koper, "Quantum-chemical calculations of CO and OH interacting with bimetallic surfaces," *Electrochim. Acta*, **47**, 3621 (2002).
33. S. Hofmann, *Auger- and X-ray photoelectron spectroscopy in materials science: a user-oriented guide*, Springer, Germany, 2013.
34. Y. X. Bai, J. J. Wu, X. P. Qiu, J. S. Wang, W. T. Zhu, and L. Q. Chen, "Preparation and performance of carbon supported platinum-tin catalyst for direct methanol fuel cell by reverse micelle method," *Acta Chim. Sinica*, **64**, 527 (2006).
35. J. M. Sieben and M. M. E. Duarte, "Nanostructured Pt and PteSn catalysts supported on oxidized carbon nanotubes for ethanol and ethylene glycol electrooxidation," *Int. J. Hydrogen Energ.*, **36**, 3313 (2011).
36. W. X. Du, G. X. Yang, E. Wong, N. A. Deskins, A. I. Frenkel, D. Su, and X. W. Teng, "Platinum-tin oxide core-shell catalysts for efficient electro-oxidation of ethanol," *J. Am. Chem. Soc.*, **136**, 10862 (2014).
37. T. Huang, R. R. Jiang, D. Zhang, J. H. Zhuang, W. B. Cai, and A. S. Yu, "AC impedance investigation of plating potentials on the catalytic activities of Pt nanocatalysts for methanol electrooxidation," *J. Solid State Electrochem.*, **14**, 101 (2010).
38. P. D. S. Correa, E. L. D. Silva, R. F. D. Silva, C. Radtke, B. Moreno, E. Chinarro, and C. D. F. Malfatti, "Effect of decreasing platinum amount in Pt-Sn-Ni alloys supported on carbon as electrocatalysts for ethanol electrooxidation," *Int. J. Hydrogen Energ.*, **37**, 9314 (2012).
39. M. J. Han, J. H. Zeng, J. W. Xia, and S. J. Liao, "Effect of thermal treatment on structural change of anode electrocatalysts for direct methanol fuel cells," *Particuology*, **15**, 45 (2014).
40. M. Zhiani, J. Jalili, B. Rezaei, and M. M. Taghiabadi, "Methanol electrooxidation on synthesized PtRu nanocatalyst supported on acetylene black in half cell and in direct methanol fuel cell," *Int. J. Hydrogen Energ.*, **38**, 5419 (2013).
41. J. Singh, R. C. Nelson, B. C. Vicente, S. L. Scott, and J. A. van Bokhoven, "Electronic structure of alumina-supported monometallic Pt and bimetallic PtSn catalysts under hydrogen and carbon monoxide environment," *Phys. Chem. Chem. Phys.*, **12**, 5668 (2010).
42. G. Y. Zhao, C. L. Xu, D. J. Guo, H. Li, and H. L. Li, "Template preparation of Pt-Ru and Pt nanowire array electrodes on a Ti/Si substrate for methanol electro-oxidation," *J. Power Sources*, **162**, 492 (2006).
43. Y. Ishikawa, M. S. Liao, and C. R. Cabrera, "Oxidation of methanol on platinum, ruthenium and mixed Pt-M metals (M = Ru, Sn): a theoretical study," *Surf. Sci.*, **463**, 66 (2000).
44. M. P. Hogarth and G. A. Hards, "Direct methanol fuel cells technological advances and future requirements," *Platin. Met. Rev.*, **40**, 150 (1996).
45. W. Tokarz, P. Piela, and A. Czerwiński, "Analysis of the influence of rhodium addition to platinum on its activity toward methanol electrooxidation by EIS," *J. Solid State Electrochem.*, **14**, 515 (2010).
46. I. M. Hsing, X. Wang, and Y. J. Leng, "Electrochemical im pedance studies of methanol electro-oxidation on Pt/C thin film electrode," *J. Electrochem. Soc.*, **5**, A615 (2002).